PHYSICAL REVIEW B VOLUME 54, NUMBER 23 15 DECEMBER 1996-I

Ballistic-electron-emission spectroscopy of Au/Si and Au/GaAs interfaces: Low-temperature measurements and ballistic models

D. K. Guthrie
Microelectronics Research Center and School of Electrical and Computer Engineering, Georgia Institute of Technology, Atlanta, Georgia 30332

L. E. Harrell
Microelectronics Research Center and School of Physics, Georgia Institute of Technology, Atlanta, Georgia 30332

G. N. Henderson*
Microelectronics Research Center and School of Electrical and Computer Engineering, Georgia Institute of Technology, Atlanta, Georgia 30332

P. N. First
Microelectronics Research Center and School of Physics, Georgia Institute of Technology, Atlanta, Georgia 30332

T. K. Gaylord and E. N. Glytsis
Microelectronics Research Center and School of Electrical and Computer Engineering, Georgia Institute of Technology, Atlanta, Georgia 30332

R. E. Leibenguth
Optoelectronics Center, Lucent Technologies Bell Laboratories, Breingsville, Pennsylvania 18031

(Received 18 December 1995; revised manuscript received 14 August 1996)

Low-temperature ballistic-electron-emission spectroscopy measurements are presented for Au/Si(100), Au/Si(111), and Au/GaAs(100) interfaces. Spectra were acquired at 77 K for the Au/Si systems and at 7 K for Au/GaAs(100). The results show that in the near-threshold region, the experimental spectra cannot be adequately described by ballistic models based only on kinematical constraints. In this work, a dynamical ballistic model is formulated incorporating the quantum transmittance and elastic scattering. The model includes all kinematically allowed semiconductor states, i.e., both zone-centered energy-band minima and non-zone-centered minima. Appropriate expressions for the quantum transmittance and reflectance functions are derived for non-zone-centered minima within a semiclassical model. Additionally, the effect of nonparabolic bands on the model is analyzed. For Au/Si(111), fits to experimental spectra show that substantial scattering must occur to account for both the observed magnitude and shape of the spectrum. For all interfaces, excellent agreement between model and experiment was obtained over a range from well below threshold up to 0.25 V above threshold, depending on the interface. The addition of an energy-dependent effective mass did not change these results. Model fits also were consistently better than previously used power-law approximations. [S0163-1829(96)03648-X]

I. INTRODUCTION AND MOTIVATION

The need for decreasing device dimensions, increasing speeds, and increasing levels of integration has focused attention on ‘‘quantum’’ devices as a new paradigm for the electronics industry. These devices can no longer be described by drift and diffusion equations, but rather rely upon electron-wave interference effects or quantum confinement for their functionality. Understanding ballistic transport of electrons and holes through these devices, determining the electronic structure near the defining interfaces, and quantifying the role of scattering, are all essential steps toward more effective device designs. Some of these issues can be addressed successfully through *ab initio* calculation, but there remains a need for semiclassical models that mesh strongly with intuition, and an even greater need for techniques that can measure the relevant properties of interfaces. The purpose of this paper is to examine the successes and limitations of a semiclassical model for one of the most promising recent characterization techniques, ballistic-electron-emission spectroscopy (BEES). A report has been given previously for the case of Au/Si(100) Schottky interfaces.[1] Here that model is expanded and compared to low-temperature measurements for Au/Si(111), Au/GaAs(100), and Au/Si(100).

BEES is a technique that uses a scanning tunneling microscope (STM) to inject hot electrons through a thin metallic base layer, and subsequently into a semiconductor collector. It has been recognized as a promising tool for characterizing quantum devices,[2–4] allowing detailed analysis of subsurface electronic properties in metal-semiconductor[1,5–12] and semiconductor-semiconductor[2–4,13] heterostructures via measurements of electron or hole transmission through the device. BEES provides nanometer-scale spatial resolution and has an energy resolution of approximately $3.5k_BT$, where k_B is Boltzmann's constant and T is the absolute temperature. The energy resolution is determined by thermal broadening of the Fermi-Dirac distribution. Current models provide good general agreement with existing experimental data,[14–22] but the limits of BEES as an analytical tool cannot be reached without a thorough understanding of the range of applicability of various models, and the relative magnitudes of elastic and inelastic processes. These issues have been addressed by others,[16,19] and BEES models exist that parametrize the effects of inelastic scattering in the base layer[19] and impact ionization in the semiconductor at higher energies.[20,22] However, for the purpose of characterizing quantum devices, it is the low-energy regime (generally much less than 0.5 eV above threshold) that is of primary interest. At the BEES threshold, where the kinetic energy of the transmitted carrier approaches zero, the ballistic component must dominate the transmitted current since carriers that have undergone inelastic collisions will fall below the threshold energy and will not be transmitted. Therefore, the approach taken in the present work is to implement first a ballistic model, and then to determine the energy range over which the model accurately describes the experimental spectra. The energy at which the model fails provides the upper bound for the validity of the underlying assumptions.

To implement this model, wave transmission across a boundary must be understood. The ideal process is often separated into two parts, although both are necessary for a consistent description of the transmission/reflection process. *Phase* effects determine the allowed trajectories of the incident and reflected waves, while *amplitude* effects determine the probability of each trajectory. In electromagnetic optics, for example, phase matching gives rise to Snell's laws of reflection and refraction, whereas amplitude matching determines the Fresnel coefficients for the reflected and transmitted amplitudes. These concepts can be generalized as *kinematical* and *dynamical* effects, respectively, thus retaining their utility even for boundaries that are not ideal planar interfaces. For the present case of electron transmission across a metal/semiconductor interface, the ''quantum transmittance'' is analogous to that in electromagnetic optics (transmitted flux/incident flux), and arises from wave-function amplitude matching. Quantitative analogies have been previously derived between electromagnetic-wave propagation in general dielectrics and electron-wave propagation in semiconductors,[23] where the effective mass approximation is known to be reliable. These analogies show that the electron-wave ''indices of refraction'' (and consequently the quantum transmittance) are functions of both the electron kinetic energy and its effective mass. At issue is whether BEES measurements are sufficiently sensitive to detect the energy-dependent quantum transmittance, and whether a semiclassical ballistic model can provide an accurate description of the quantum transmittance for a metal/semiconductor interface.

In practice, the effect of the quantum transmittance might be rendered unobservable for several reasons: (1) The BEES current resulting from electron transmission is summed over all incident angles and all injected energies. Thus phase space restrictions on these sums largely determine the spectral shape, which can mask the less obvious influence of the quantum transmittance. (2) The transmittance function may approach unity within an energy range smaller than the experimental resolution, or conversely its intrinsic energy dependence may be too weak to be observable. (3) Scattering events may redistribute the incident electron flux into different angles (elastic or inelastic scattering) or into different energies (inelastic scattering). Either could impart a substantial energy dependence to the spectrum that might overwhelm the effect of the quantum transmittance. For instance, Monte Carlo calculations by Lee and Schowalter[17] suggest that energy variation in the quantum transmittance is quickly canceled by the energy-dependent cross section for optical-phonon scattering in the semiconductor. Accurate, high-resolution spectra are required to overcome the first two issues. The third is difficult to address directly, but a comparison of experimental spectra to a ballistic model will determine the energy above which inelastic events affect the spectral shape.

Semiclassical models that rely on the effective-mass approximation have proven to be so useful and intuitive in semiconductor physics that they are often applied to cases where the approximations of the model are not strictly valid.[24] Nonetheless, model predictions in these instances are often quantitatively confirmed by experiment.[25] For ballistic transmission through a metal/semiconductor interface, some of the assumptions are indeed violated, yet it is worthwhile to examine a semiclassical model for the quantum transmittance because (a) it is tractable and (b) it is easily integrated into a calculation of the total transmittance through a collector composed of a semiconductor heterostructure device. Previous studies have recognized the importance of ''off-axis'' band minima,[14–16] but have not included the effects of angle and the energy dependence of the transmittance into these states. In this work we have implemented a semiclassical model that includes the effects of quantum transmittance into all kinematically allowed states of the semiconductor.

The remainder of the paper is organized as follows: Section II describes the ballistic model for the quantum transmittance and the chosen form of the electron distribution incident on the interface. In Sec. III, model results are interpreted and compared to experimental spectra. The effects of elastic scattering, the quantum transmittance, and nonparabolicity are determined in this section. Finally, Sec. IV provides a summary and conclusions.

II. THEORY

A. Introduction

In this section we describe a model that incorporates the amplitude effects in the near-threshold region, in addition to phase constraints. The amplitude effects are embodied in the quantum transmittance and in elastic-scattering events, which change the incident electron trajectories. The phase effects determine the electron states that are available for transmission. We first discuss the limitations and utility of the model, and then pursue the details.

The model presented below relies upon a single-band effective-mass theory and the envelope wave-function approximation[24] to calculate the quantum transmittance through a metal/semiconductor interface. The interface is assumed to be abrupt, and the metal is taken to be nearly free electron, as has been the case for most other models of BEES.[6,14] The boundary conditions that rely on matching envelope wave functions are valid only if the central cell portions of the total wave functions are identical. This is not the case for different materials. Furthermore, the interfaces considered here are typically not as abrupt as epitaxial semiconductor/semiconductor interfaces, where these approximations have been quite successful. Interdiffusion, possible passivation or contamination layers, and image charge effects all affect the width of the transition region between bulk metallic states and bulk semiconductor states. Finally, although there are clear similarities above the Fermi level E_F, the band structure and wave functions of Au deviate markedly from free-electron behavior. This is most apparent near the $\langle 111 \rangle$ directions, where there are regions with no propagating states.

Having listed the approximations, it is worthwhile to examine where the model is valid. First, within the single-band approximation, the model employs the correct phase space for the semiconductor, and nearly so for the metal. It is the number of states available for transmission that plays the primary role in determining the BEES spectral shape. Second, and of most interest here, the calculated quantum transmittance has the correct form in both the low-energy and high-energy limits. Provided the energy of the incident electron is sufficiently far from a band extremum in the metal (so that the incident electron flux density may be considered constant over a small energy range), the transmittance near threshold will be proportional to the normal component of the group velocity in the collector, which itself varies as $E^{1/2}$ (i.e., $[V-V_b]^{1/2}$, where V is the magnitude of the tunnel voltage and V_b is the Schottky barrier height) at a band extremum. At high energies the transmittance must saturate to a constant value for a parabolic band. For real materials saturation may not be reached before the bands become nonparabolic, but even so, the energy dependence of the transmittance becomes substantially weaker at higher energies. These conclusions will not be dramatically affected by details of the metal/semiconductor transition region, such as image potential lowering, so long as inelastic effects are negligible and the relative change in kinetic energy is large. We expect, therefore, that an effective mass model will produce an accurate model for the transmittance through a simple metal/semiconductor interface.

B. Quantum transmittance

The quantum transmittance can be calculated by assuming that the Schottky barrier forms a step potential with differing effective mass on either side. Under the single-band, time-independent effective-mass approximation, the quantum transmittance of an abrupt potential barrier can be determined in closed form. Many textbooks derive this result for the zone-centered case,[24] but omit non-zone-centered minima. The quantum transmittance into non-zone-centered band minima is needed to treat materials like silicon. In this work, the quantum-mechanical transmittance and reflectance for an interface between two arbitrary material systems is developed. The resulting expression applies to both zone-centered and non-zone-centered minima.

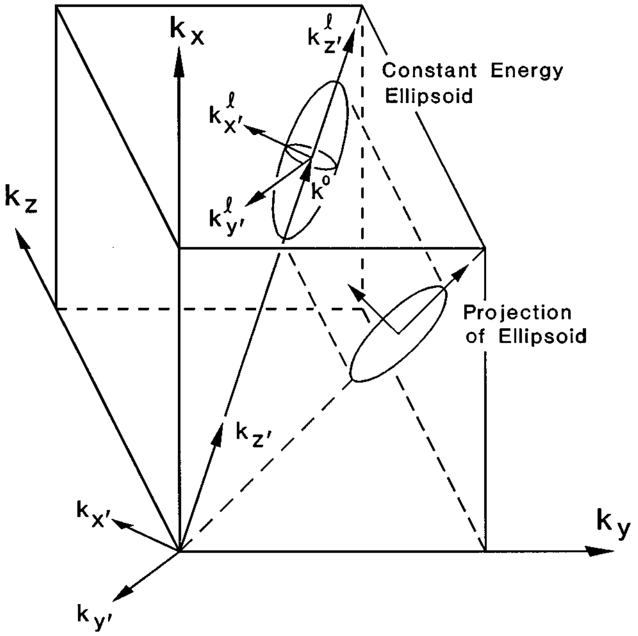

FIG. 1. An ellipsoidal constant-energy surface in momentum space. The ellipsoid has been rotated from the principal coordinate system ($k_{x'}$, $k_{y'}$, $k_{z'}$) into an interface coordinate system (k_x, k_y, k_z) and projected onto the interface plane. The projection represents the allowable momentum states into which an electron can be transmitted.

Consider an electron in the base material incident upon an interface with the collector material. The incident electron wave vector in the base can be expressed as the sum of a ‘‘local’’ wave vector, $\mathbf{k}^{\ell}_i$, and $\mathbf{k}^0_B$, the wave vector which locates the appropriate band minimum. The wave vectors of both the reflected and transmitted wave functions can be written similarly, although the band offset in the collector, $\mathbf{k}^0_C$, will generally be different than that in the base. To satisfy conservation of energy, only those wave vectors lying on ellipsoidal constant energy surfaces,

$$E(\mathbf{k}^{\ell})=E^0+\frac{\hbar^2}{2}(\mathbf{k}^{\ell})\mathbf{M}^{-1}(\mathbf{k}^{\ell})^T, \tag{1}$$

can be considered. Here $\mathbf{M}^{-1}$ is the inverse effective-mass tensor for the material, superscript T denotes vector transpose, and E^0 is the energy of the relevant band minimum.

Conservation of momentum parallel to the interface plane (‘‘phase matching’’) determines the set of wave vectors for which the electron can possibly be transmitted. As shown in Fig. 1, the projection of a constant energy surface ($k_{x'}$, $k_{y'}$, $k_{z'}$) onto the interface plane (k_x, k_y, 0) determines all of the parallel wave vectors that are energetically allowed. The overlap of projections from the base and collector constant energy surfaces then gives the set of wave vectors that obey both conservation of energy and conservation of parallel momentum. To find the required projections and overlap, we evaluate Eq. (1) (for both base and collector) in the ‘‘interface coordinate system’’ defined by the interface normal, $\hat{\mathbf{z}}$, and a convenient choice of orthogonal $\hat{\mathbf{x}}$ and $\hat{\mathbf{y}}$ in the interface plane. The inverse effective-mass tensor in the interface coordinate system is expressed in the principal axis system via a unitary transformation as

$$\mathbf{M}^{-1}=\mathbf{\Theta}\mathbf{M}_D^{-1}\mathbf{\Theta}^T, \tag{2}$$

where $\mathbf{M}_D^{-1}$ is the principal axis (diagonal) representation of the tensor, and $\mathbf{\Theta}$ is the rotation matrix that transforms from principal axis coordinates to the interface coordinate system. For the usual case, the set of projected wave vectors in the base encompasses all of those in the collector, so that the overlap is simply determined by the projections of the collector constant energy surfaces.

Given the states for which electron transmission is allowed, the quantum transmittance may be calculated by applying the appropriate boundary conditions. However, modifications for the case of non-zone-centered band minima are necessary. For nondegenerate conduction-band minima we define the envelope wave functions on the base (B) and collector (C) sides of the interface as[26]

$$\psi_B=\psi_B^{\ell}\psi_B^0=(e^{i\mathbf{k}_i^{\ell}\cdot\mathbf{r}}+re^{i\mathbf{k}_r^{\ell}\cdot\mathbf{r}})(e^{i\mathbf{k}_B^0\cdot\mathbf{r}}), \tag{3}$$

$$\psi_C=\psi_C^{\ell}\psi_C^0=(te^{i\mathbf{k}_t^{\ell}\cdot\mathbf{r}})(e^{i\mathbf{k}_C^0\cdot\mathbf{r}}). \tag{4}$$

The first boundary condition, continuity of the wave-function amplitude at the interface, yields the phase matching conditions already applied and the relation $t=1+r$. For a zone-centered minimum, the second boundary condition commonly used is the continuity of $(1/m_z^*)\hat{\mathbf{z}}\cdot\mathbf{\nabla}\psi$. For a non-zone-centered minimum it can be shown from $\mathbf{k}\cdot\mathbf{p}$ perturbation theory that the second boundary condition must be calculated using the wave vector relative to the band minimum, $\mathbf{k}^{\ell}$, since the group velocity is determined by $\mathbf{k}^l$.[27] The second boundary condition may then be written for an arbitrary interface at $z=0$ as

$$\hat{\mathbf{z}}\cdot(\mathbf{M}_B^{-1}\mathbf{\nabla}\psi_B^{\ell})|_{z=0}=\hat{\mathbf{z}}\cdot(\mathbf{M}_C^{-1}\mathbf{\nabla}\psi_C^{\ell})|_{z=0}, \tag{5}$$

where $\hat{\mathbf{z}}$ represents the unit vector normal to the interface. It is easily shown that this condition implies continuity of the average current. Defining $\alpha=\hat{\mathbf{z}}\cdot(\mathbf{M}_B^{-1}\mathbf{k}_i^{\ell})$ and $\gamma=\hat{\mathbf{z}}\cdot(\mathbf{M}_C^{-1}\mathbf{k}_t^{\ell})$, the complex reflection and transmission amplitude coefficients r and t are given by

$$r=\frac{\alpha-\gamma}{\alpha+\gamma}, \tag{6}$$

$$t=\frac{2\alpha}{\alpha+\gamma}. \tag{7}$$

The transmittance and reflectance are the fractions of transmitted and reflected current,

$$T=\frac{J_t}{J_i}=\frac{\gamma}{\alpha}|t|^2, \tag{8}$$

$$R=-\frac{J_r}{J_i}=|r|^2. \tag{9}$$

We emphasize once more that the model is valid for the case of a single band associated with each minimum. In a multiple-band treatment the allowed phase space will include states at the same parallel component of crystal momentum, but corresponding to different Bloch states. The quantum transmittance into these states will depend on the interband coupling. For the case of Si, one might expect the interband coupling to become quite large when the constant energy surfaces approach the Brillouin-zone boundary at the X point ($V-V_b\sim0.1$ V). Fortunately, the structure factor of the Si crystal potential is zero for the (200) Fourier component, so that the ellipsoids are continuous across the zone boundary.

C. Electron distribution

Scattering in the base and at the interface may also affect the shape of the spectrum. For the near-threshold region, most inelastic-scattering events will reduce the electron energy to a value below the Schottky barrier. Consequently, only the effect of elastic scattering on the distribution will be included here. Elastic scattering may be modeled by considering a fraction s of the incident electrons to be scattered isotropically. The distribution incident on the interface is then

$$D_C(E,k_\parallel)=(1-s)D_T(E-eV,k_\parallel)+sD_s(E,k_\parallel), \tag{10}$$

where $k_\parallel^2=k_x^2+k_y^2$ is the component of the incident wave vector parallel to the interface plane, $D_T(E,k_\parallel)$ is the planar tunneling distribution, V is the magnitude of the tip-base potential difference, $-e$ is the electron charge, and $D_s(E,k_\parallel)$ is an isotropic distribution with an equal number of electrons at all angles of incidence θ_i, where $\tan\theta_i=k_\parallel/k_z$. The isotropic distribution $D_s(E,k_\parallel)$ is determined by the requirement that the number of electrons is conserved in the scattering. Thus

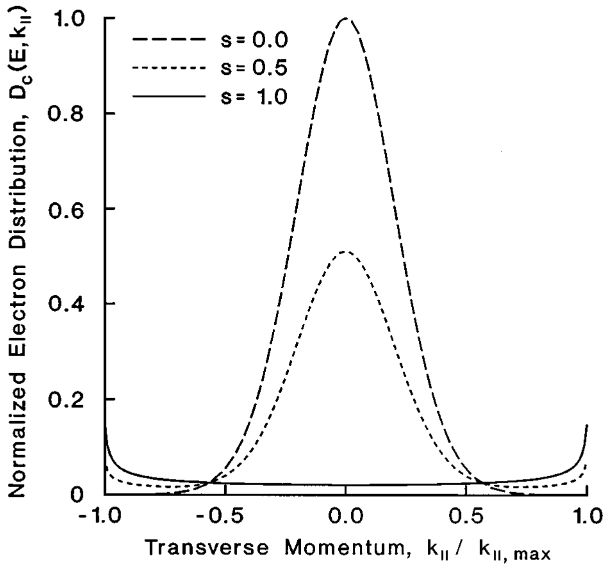

FIG. 2. The electron distribution incident upon the base-semiconductor interface corresponding to various values of s. The distribution was varied from a planar tunneling distribution ($s=0$) to an isotropic distribution ($s=1$) to account for elastic scattering in the base and at the interface.

$$D_s(E,k_\parallel)=\frac{1}{|\mathbf{k}_i|^2\sqrt{1-k_\parallel^2/|\mathbf{k}_i|^2}}\left(\int_0^{|\mathbf{k_i}|}k_\parallel D_T(E-eV,k_\parallel)dk_\parallel\right), \tag{11}$$

where $\mathbf{k}_i$ is the incident wave vector. Figure 2 shows the distribution for various values of s ranging from planar tunneling ($s=0$) to isotropic ($s=1$). Note that the parallel component of momentum is still conserved at the interface. In the model, scattering occurs *before* wave-function matching.

D. Model

A BEES model can now be formulated that includes elastic scattering and the quantum transmittance for zone-centered as well as non-zone-centered minima. For a single-band minimum, the ratio of collector current I_C to tunnel current I_T is given by

$$\left(\frac{I_C}{I_T}\right)_i=\mathcal{R}\,\frac{\int_{E_{f+eV_b}}^{\infty}f(E-eV)\int\int D_C(E,k_x,k_y)T(E,k_x,k_y)dk_ydk_xdE}{\int_{eV}^{\infty}[f(E-eV)-f(E)]\int\int D_T(E-eV,k_x,k_y)dk_ydk_xdE}, \tag{12}$$

where E is measured from the bottom of the conduction band in the base. D_T is the planar tunneling distribution and D_C the electron distribution incident on the collector. The quantum transmittance is denoted by T, $f(E)$ is the Fermi function, V_b is the Schottky barrier height, and $\mathcal{R}$ is an energy-independent scale factor accounting for attenuation in the base. The subscript i labels the particular band minimum under consideration. The limits of integration in k_x, k_y are determined by the projections of the constant energy ellipsoids onto the interface plane as shown in Fig. 1.

The model defined by Eqs. (6)–(12) will be referred to as the $T(E)$ model for brevity, even though the k_x, k_y dependence of the quantum transmittance has been included in the calculations. In Sec. III C the $T(E)$ model will be compared with a simplified model obtained by setting the transmittance to unity in Eq. (12), for all energies and angles. This will be called the $T=1$ model. The $T(E)$ model has been used for all calculations, except those in Sec. III C that are labeled otherwise.

III. RESULTS

A. Introduction

As discussed in Sec. I, the overall shape of the BEES spectrum for a simple Schottky interface is largely determined by the number of states available for transmission into the semiconductor. The additional influence of the quantum transmittance is quite subtle, thus in order to resolve it, one must acquire high-resolution spectra with very high signal-to-noise ratio. To meet these requirements, a BEES apparatus was constructed for operation down to temperatures as low as 6–7 K.[28] The inherent BEES energy resolution is expected to be 2.1 meV at 7 K and 23 meV at 77 K (the two temperatures relevant to this work), and the noise level in some of the measurements presented here was as low as a few fA. Also, because of the low drift rate inherent in the STM, the tip remained at the same position to within a few Å during acquisition of a spectrum. This is an important aspect of the measurements, since small shifts in the threshold voltage from one spatial position to another would otherwise degrade the resolution. Au/Si(100) and Au/Si(111) diodes were phosphorous-doped 1×10^{15} cm^{-3} and 1×10^{16} cm^{-3}, respectively, and were prepared for evaporation by cleaning in trichloroethylene, acetone, and dehydrated ethanol followed by etching in a 10:1 ethanol:HF solution for 90 sec. GaAs samples consisted of a 1-μm-thick layer of n-type (Si-doped, 1×10^{15} cm^{-3}) grown by MBE on a degenerate n-GaAs substrate. Wafers were capped with arsenic before removal from the growth chamber. Before diode preparation, the arsenic cap was removed by electron-beam heating to 400 °C in vacuum. The sample was cooled and removed from the vacuum, then passivated in $NH_4(OH)$ for 30 sec.[29] A 7-nm-thick gold base layer was deposited at room temperature by electron-beam evaporation for the Si devices and by thermal evaporation for the GaAs devices. For both cases, the background pressure was $\approx5\times10^{-7}$ torr. All Si experimental data were taken at $T=77$ K in order to avoid spectral distortions caused by the large bulk resistivity at lower temperatures.[1] The 77 K spectra were smoothed using a ten-point Gaussian with a FWHM of 7.5 meV to reduce digital noise. All GaAs experimental data were taken at 7 K. In this case the spectra were not smoothed, since the energy resolution at this temperature is smaller than the voltage step used (2.5 mV) for data acquisition. Spectra were acquired at a number of locations on each of several diodes for each interface system.

B. Electron distribution

Without the inclusion of some form of scattering, ballistic models cannot accurately predict the observed magnitude of the Au/Si(111) BEES spectrum. In the present work, the effect of elastic scattering in the base and at the interface is modeled by the distribution incident upon the base-semiconductor interface, as given by Eq. (10) and shown in Fig. 2. In what follows we first discuss the effect of elastic scattering on the predicted spectra in light of the available states in the semiconductor. Subsequently we compare model to experiment.

1. Simulation

For a fixed energy near the transmission threshold, the allowed set of interface wave vectors are drawn in Fig. 3. Parts (a)–(c) of the figure show the interface Brillouin zone and projected bulk states for Si(111), Si(100), and GaAs(100), respectively. The allowed states in Si(111) and

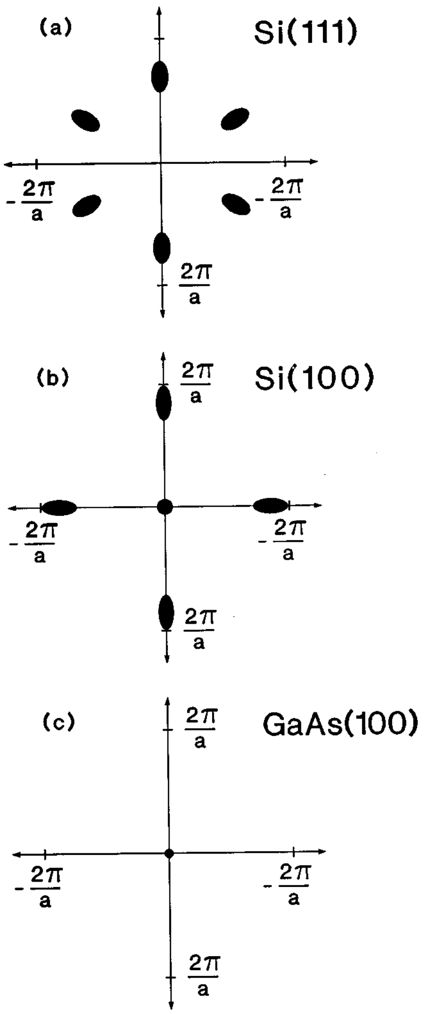

FIG. 3. Projection of the constant energy surfaces onto the interface plane. (a) For Si(111), an electron must have a large transverse momentum to phase match, implying a large angle of incidence. (b) For Si(100), electrons with both large and small transverse momenta are transmitted: (c) For GaAs, only electrons near normal incidence can be transmitted.

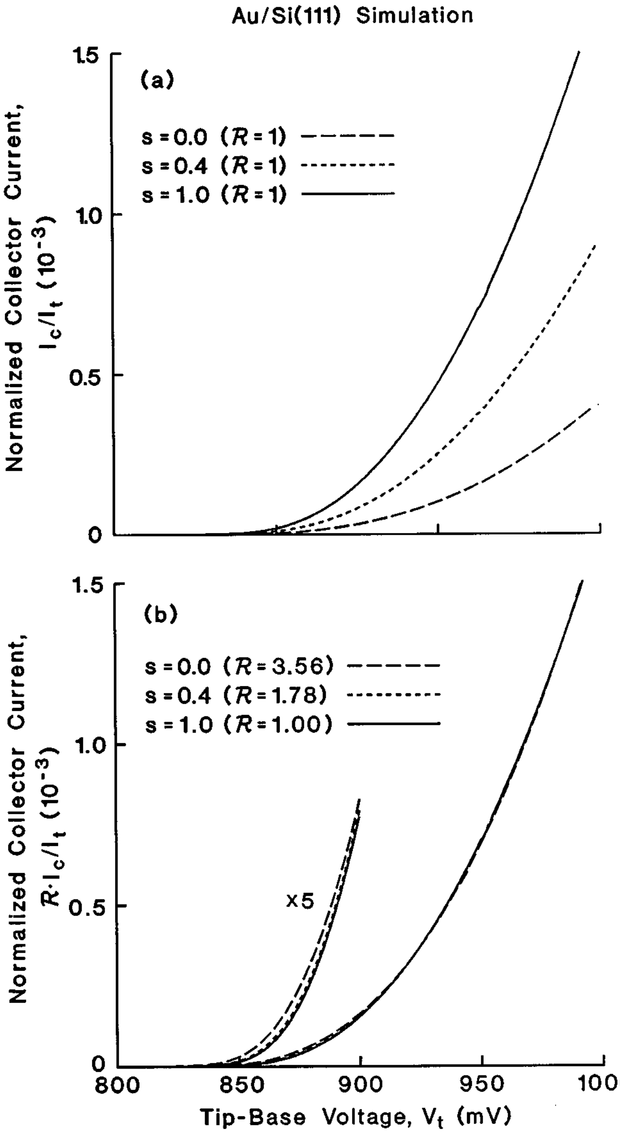

FIG. 4. Simulation of BEES current for a Au/Si(111) diode for various amounts of elastic scattering. The Schottky barrier height is 850 mV. (a) As the scattering increases, more electrons can phase match and the magnitude increases. (b) Only a small amount of scattering is needed to account for the shape of the spectrum, but considerably more is needed to account for the magnitude.

GaAs(100) are seen to be completely different. For Si(111), there are no states available for transmission at the center of the zone, while for GaAs(100) states exist only near the zone center at this energy. Elastic scattering can be expected to affect the transmitted current in opposite ways for these two cases. Si(100) provides an intermediate case, with kinematically allowed states available both at the zone center and in off-axis band minima.

Figure 4(a) shows the effect of elastic scattering on the simulated Au/Si(111) BEES spectrum calculated using the $T(E)$ model. The amount of scattering increases as the parameter s varies from 0 to 1 [see Eq. (10)], and $\mathcal{R}$ is the scale factor applied to the spectrum. Notice that the simulated current increases with increasing scattering. This is consistent with the geometry of the allowed states in the semiconductor, as pictured in Fig. 3(a) and previously recognized by others.[15] Figure 4 compares the shapes of spectra simulated with different levels of elastic scattering by adjusting the scale factor $\mathcal{R}$ to obtain a best fit among them. The magnified region shows that near the BEES threshold the $s=0$ spectral shape is noticeably different from that for isotropic scattering ($s=1$). However, even a small amount of scattering quickly drives the shape toward that of isotropic scattering.

Scattering-induced changes in the simulated spectra are not as large for Au/Si(100) as those predicted for Au/Si(111). Significantly, Fig. 5(a) shows that elastic scattering reduces the magnitude of the current. This seems to contradict the observation that there are many more states in the off-axis ellipsoids (reached by scattering) than in the small zone-centered minima. Note that scattering spreads the electrons over all angles, however. Therefore the fraction of electrons incident at angles that can phase match into Si(100) is reduced [cf. Fig. 3(b)] and the current decreases. Changes of the spectral shape with increased elastic scattering are less pronounced for Au/Si(100), as seen in Fig. 5(b).

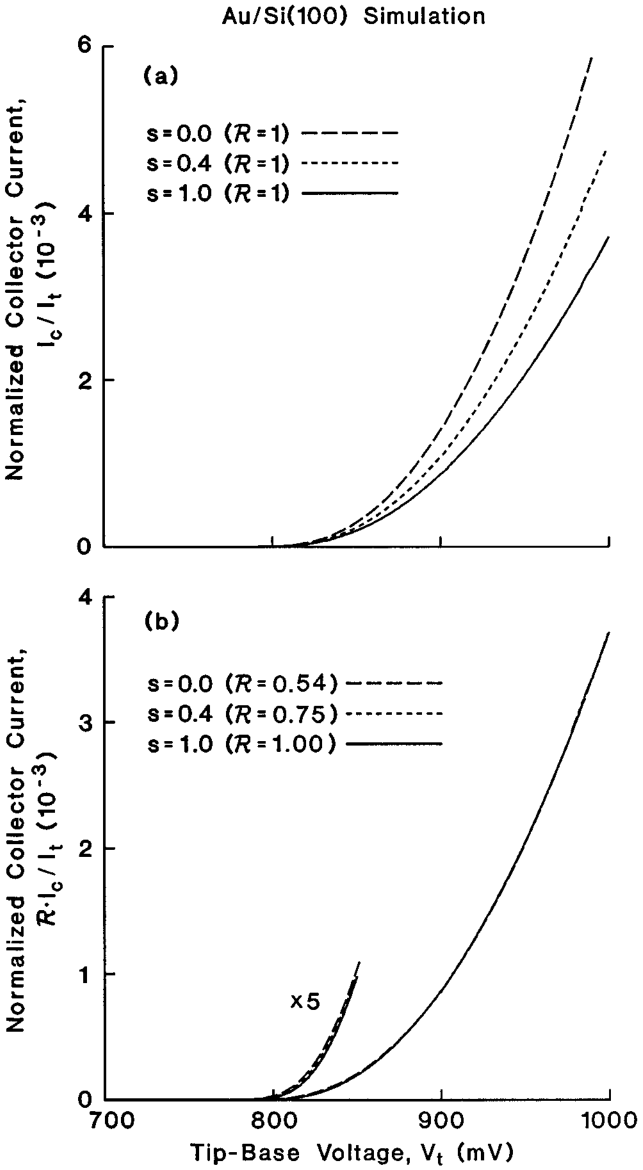

FIG. 5. Simulation of BEES current for a Au/Si(100) diode for various amounts of elastic scattering. The Schottky barrier height is 800 mV. (a) As s increases, electrons are shifted from directly over the zone-centered band minima to larger values of $k_{\parallel}$ where the ratio of transmitting states to nontransmitting states is smaller. Consequently the magnitude decreases and the shape (b) changes slightly.

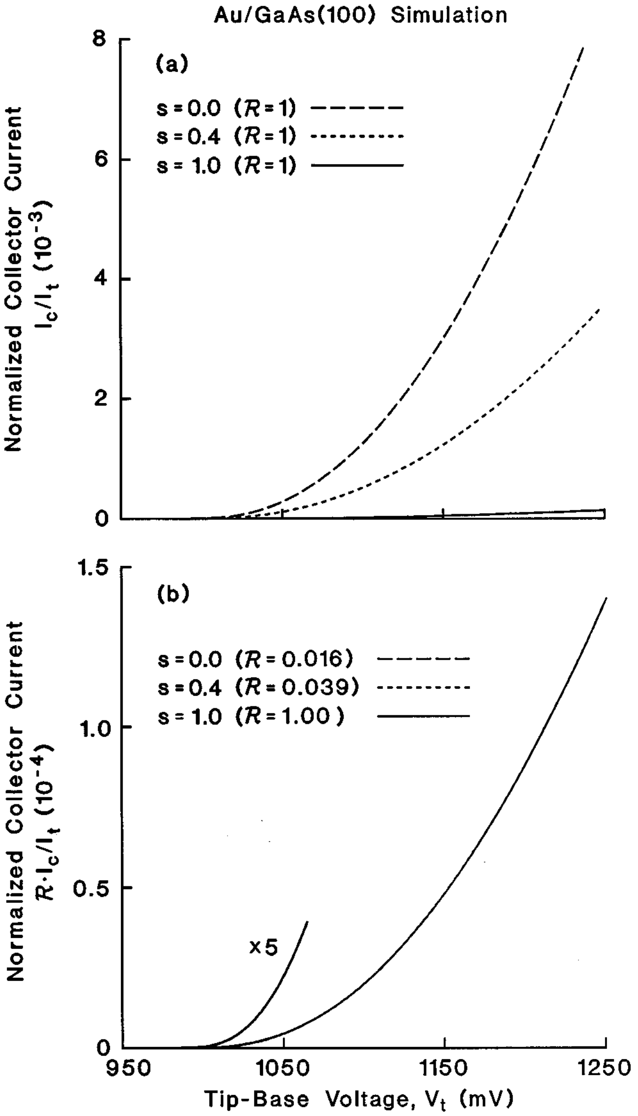

FIG. 6. Simulation of BEES current for a Au/GaAs(100) diode for various amounts of elastic scattering. The Schottky barrier height is 1000 mV. (a) As scattering increases, the magnitude decreases, but (b) the shape of the spectrum is completely independent of the scattering (all curves lie on top of each other).

For Au/GaAs(100), Fig. 6(a) shows that changes in the magnitude of the simulated BEES current are more dramatic than either of the previous two cases. In this case the current decreases with increasing s because electrons are scattered away from the zone center. This behavior is opposite that observed for Au/Si(111) simulations, as anticipated from the phase-space plots of Fig. 3. Essentially no change in the shape of the simulated spectrum is observed for Au/GaAs(100) at any level of scattering, as seen in Fig. 6(b). Since the region of allowed wave vectors is so small, the distribution is always nearly uniform across it. Thus only the magnitude of the current can change significantly.

2. Experiment

Experimentally, the effect of varying the incident distribution can be seen in the quality of the model fits as determined by the mean-squared error, σ^2, and to a lesser extent the value of the scale factor, $\mathcal{R}$. A value of $\mathcal{R}>1$ indicates that the experimental spectrum has a greater magnitude than the simulation. Table I summarizes the results of fitting the experimental spectra to simulations employing various values of s.

For Au/Si(111), Table I shows that as more elastic scattering is introduced, the goodness of the fits to the simulations improves (σ^2 decreases). This indicates that a substantial amount of scattering is required to obtain the correct spectral shape. From the behavior of σ^2 it appears that $s \geqslant 0.5$. Note that the value of $\mathcal{R}$ remains greater than 1 for all s. This would seem to be unphysical since inelastic scattering should always reduce the current. Recent measurements of a 100-nm inelastic mean free path in Au (Ref. 30) may provide an explanation, however. For the 7-nm-thick films employed in this work, one would expect to get multiple reflections from the metal/vacuum interface, thus each

TABLE I. Results of fitting simulatioins with various values of s to Au/Si(111), Au/Si(100), and Au/GaAs(100) spectra. The mean-squared error, σ^2 (10^{-5} pA^2), indicates the goodness of the fit with respect to the shape, and $\mathcal{R}$ an energy-independent scale factor, indicates the magnitude of the simulation with respect to the experimental spectra. The upper fit voltages used to fit the data were 949 mV, 986 mV, and 1262 mV for Si(111), Si(100), and GaAs(100), respectively. The lower fit voltages were fixed 100 mV below threshold.

		Fraction of electrons scattered, s					
		0.0	0.2	0.4	0.6	0.8	1.0
Si(111)	$\mathcal{R}$	7.871	4.836	3.481	2.717	2.227	1.887
	σ^2	3.723	1.927	1.521	1.383	1.327	1.302
Si(100)	$\mathcal{R}$	0.533	0.586	0.651	0.733	0.835	0.972
	σ^2	8.776	7.170	5.855	4.203	3.479	3.518
GaAs(100)	$\mathcal{R}$	0.028	0.036	0.047	0.070	0.135	1.806
	σ^2	0.659	0.659	0.658	0.659	0.658	0.652

electron may have several opportunities to be transmitted. Another possible explanation is related to the assumption that the Au base is free-electron-like. The band structure of Au has ''necks'' of nonpropagating states in the ⟨111⟩ directions, which are also the preferred growth directions in the absence of any epitaxial relationship (due to close packing). This would imply that the initial distribution is not forward peaked as assumed for the ordinary planar tunneling case. Instead, the incident distribution may have no electrons at normal incidence (in the ⟨111⟩ direction), thus more of the weight of the distribution would be at large angles, where Si(111) has allowed wave-vector states.[31] As a result, the collector current would be somewhat higher than for tunneling into a free-electron metal. This scenario seems unlikely to account for the full discrepancy in $\mathcal{R}$ however. Multiple reflections appear to be the most likely explanation, although interband coupling would also contribute to larger $\mathcal{R}$ values.

For Au/Si(100), Table I shows that a nearly isotropic distribution minimizes the error and provides the correct shape. For this case as for Au/Si(111), the values of σ^2 appear to stabilize for $s \geqslant 0.5$. The magnitude of $\mathcal{R}$ is again quite large for large s (where the spectral shape is best reproduced) and we once more speculate that multiple reflections from the metal/vacuum interface may be the reason.

For Au/GaAs(100), $\mathcal{R}$ becomes extremely small for simulations with a planar tunneling distribution, and begins to obtain more realistic values for $s > 0.8$. The error in the fit remains constant as s is increased, indicating again that the Au/GaAs(100) simulation shape is unaffected by the amount of scattering. Because the shape does not change with s, it is

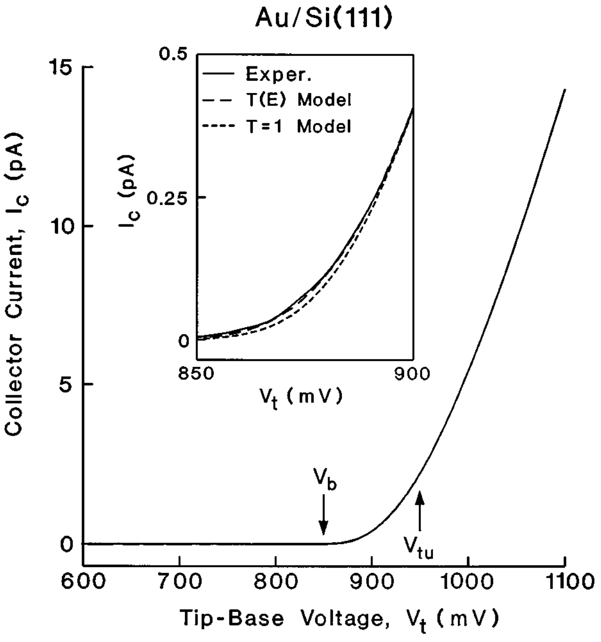

FIG. 7. $T(E)$ and $T=1$ models fit to an experimental Au/Si(111) spectrum (2-nA tunnel current, temperature 77 K). V_b labels the Schottky barrier height and V_{tu} is the upper voltage of the fitting range. The inset shows the threshold region, where ballistic models are valid. In this region the $T(E)$ model fits the data better than the $T=1$ model.

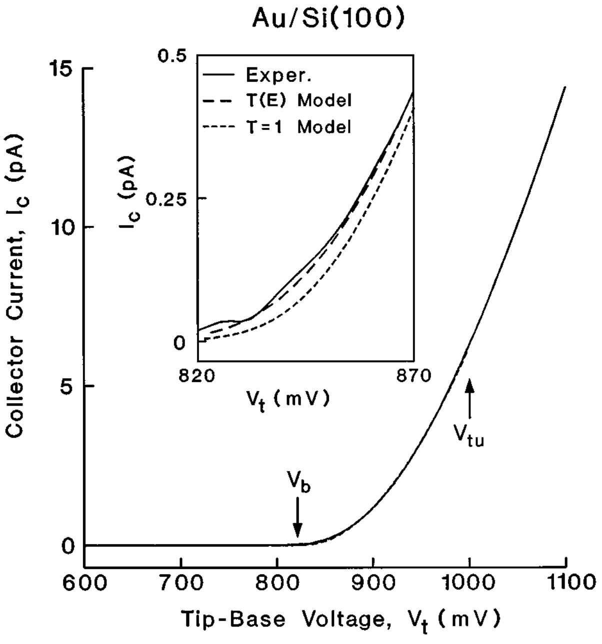

FIG. 8. $T(E)$ and $T=1$ models fit to an experimental Au/Si(100) spectrum (2-nA tunnel current, temperature 77 K). V_b labels the Schottky barrier height and V_{tu} is the upper voltage of the fitting range. The inset shows the threshold region, where ballistic models are valid. The $T(E)$ model produces the correct spectral shape near threshold.

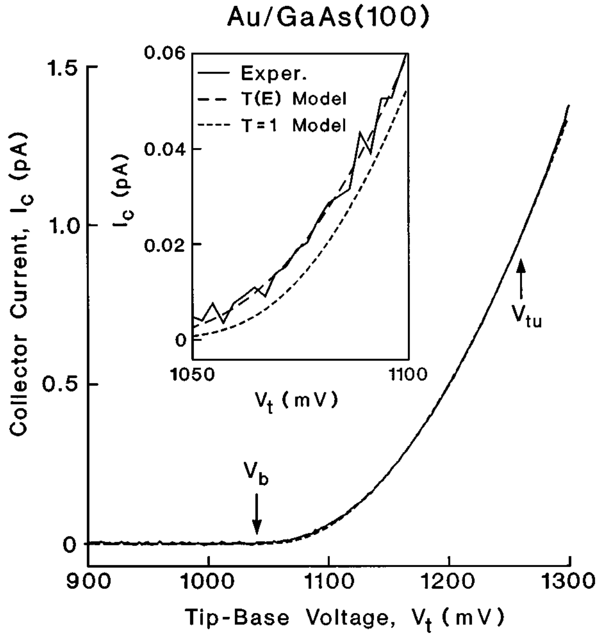

FIG. 9. $T(E)$ and $T=1$ models fit to an experimental Au/GaAs(100) spectrum (5-nA tunnel current, temperature 7 K). V_b labels the Schottky barrier height and V_{tu} is the upper voltage of the fitting range. The inset shows the threshold region, where ballistic models are valid. For this case the $T(E)$ model again gives the correct threshold shape.

difficult to determine much about the level of elastic scattering for this system. In this case it should also be pointed out that the passivation layer may reduce the value of $\mathcal{R}$.

C. Quantum transmittance

In order to reveal the effect of an energy-dependent quantum transmittance, two models [$T=1$ and $T(E)$; see Sec. II D] were fit to the experimental data. Previously, a model including quantum transmittance and a planar tunneling distribution for the zone-centered band minima of Si(100) was shown to provide a better description of measured spectra than the original BEES model,[1] which also assumed unity transmittance. The following analysis uses simulations calculated with all relevant band minima and an *isotropic* ($s=1.0$) distribution for both $T=1$ and $T(E)$ models. An isotropic distribution produces the correct shape as shown in Table I. The nonlinear-least-square fits require two free parameters, the barrier height V_b and the scale factor $\mathcal{R}$. Figures 7–12 show the results of fitting the models to the experimental data for each interface system.

Shown in Figs. 7–9 are typical experimental spectra for Au/Si(111), Au/Si(100), and Au/GaAs(100), respectively. For each interface, the data have been fit to both the $T(E)$ and the $T=1$ model up to an upper fit voltage V_{tu}. These plots show that for large voltage ranges, both models appear to provide a good description of the data. However, these models behave differently in the threshold region where a ballistic model is most valid. Shown in the insets of Figs. 7–9 are 50-mV regions just above threshold. For all three interface systems the $T(E)$ model provides a noticeably better fit than the $T=1$ model in the near threshold region.

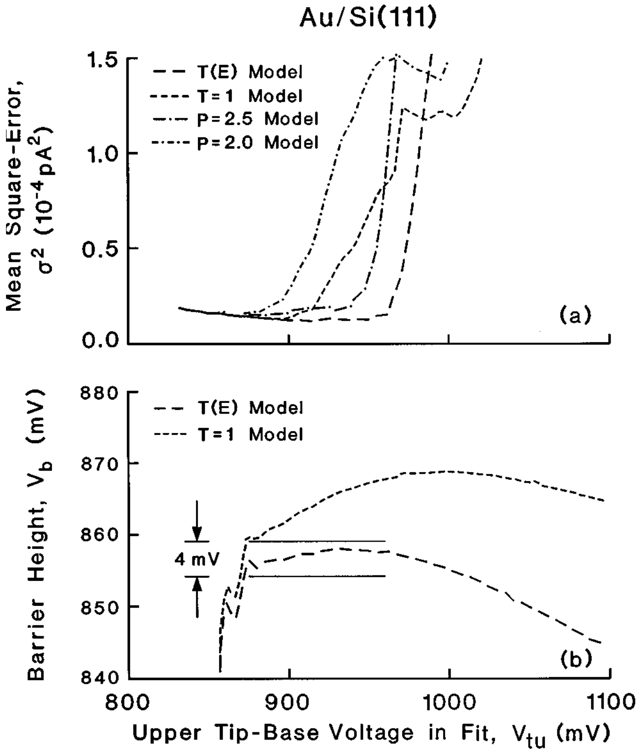

FIG. 10. (a) The mean-squared error between the experimental spectrum and the simulations plotted as a function of the upper fit voltage, V_{tu}. The $T(E)$ model provides an accurate description of the data over a range of ≈ 100 mV above threshold, whereas the $T=1$ model becomes inaccurate ≈ 30 mV above threshold. Shown for comparison are the $P=2$ and $P=5/2$ thermally broadened power laws. $P=5/2$ models the data better than $P=2$, indicating the presence of a $\sqrt{E}$ energy-dependent transmission. The superior fit of the $T(E)$ model shows that the simple $\sqrt{E}$ model for the transmission is not sufficient. (b) The barrier height as a function of upper fit voltage. The barrier height for the $T(E)$ model varies by less than 4 mV and the $T=1$ model varies by more than 12 mV over the threshold region.

To illustrate that the $T(E)$ model provides a correct description of the spectral shape and to evaluate its range of validity, a plot of the error of the fit versus fit range was calculated. This is determined by evaluating the mean-squared error between the data and the simulation for many different fitting ranges. The lower voltage is fixed well below the threshold, and the upper fit voltage V_{tu} is varied. The error vs fit range and barrier height vs. fit range plots for Au/Si(111), Au/Si(100), and Au/GaAs(100) are shown in Figs. 10–12. These plots show that, over the threshold region, the $T(E)$ model accurately describes the data in a stable fashion. The plots also show that the $T=1$ model, which neglects the energy dependence of the transmittance, does not accurately describe the data, and fits more poorly as the fit range is increased. The range of validity for each interface system can be determined from these plots. For the best case of Au/GaAs(100) [Fig. 12(a)] the $T(E)$ model is accurate up to approximately 250 mV above threshold. This covers almost the entire energy range up to the next band minima at the L points. The worst case occurs for Au/Si(111) [Fig. 10(a)] where the range of validity still extends 100 mV above threshold.

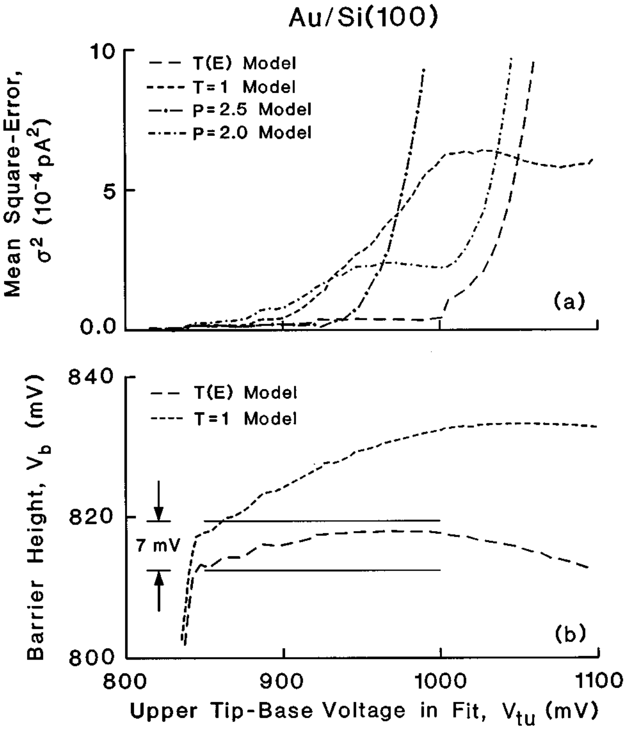

FIG. 11. (a) The mean-squared error between the experimental spectrum and the simulations is plotted as a function of the upper fit voltage, V_{tu}. The $T(E)$ model provides an accurate description of the data over a range of ≈170 mV above threshold whereas the $T=1$ model becomes inaccurate ≈60 mV above threshold. Shown for comparison are the $P=2$ and $P=5/2$ thermally broadened power laws. (b) The barrier height as a function of upper fit voltage. The barrier height for the $T(E)$ model varies by less than 7 mV and the $T=1$ model varies by more than 17 mV over the threshold region.

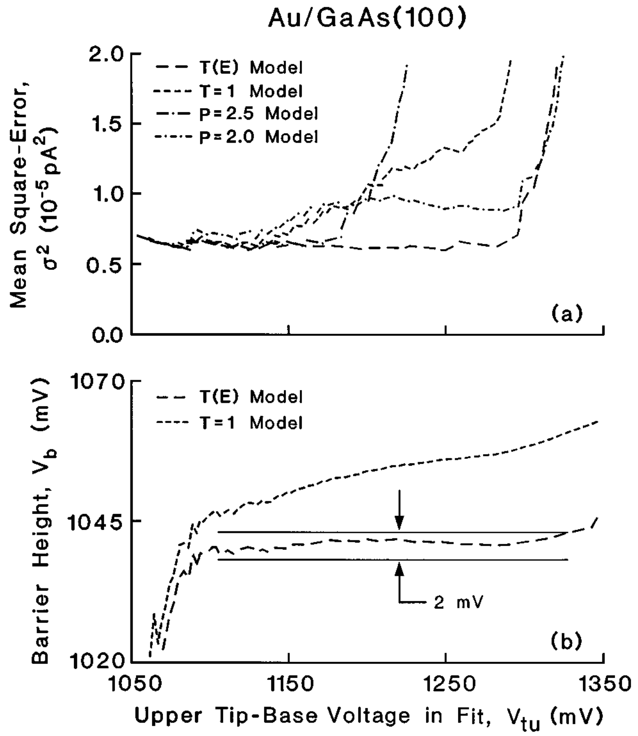

FIG. 12. (a) The mean-squared error between the experimental spectrum and the simulations is plotted as a function of the upper fit voltage, V_{tu}. The $T(E)$ model provides an accurate description of the data over a range of ≈250 mV above threshold, whereas the $T=1$ model becomes inaccurate ≈100 mV above threshold. Shown for comparison are the $P=2$ and $P=5/2$ thermally broadened power laws. (b) The barrier height as a function of upper fit voltage. The barrier height for the $T(E)$ model varies by less than 2 mV and the $T=1$ model varies by more than 10 mV over the threshold region.

Figures 10–12 also show the error vs fit range for thermally broadened $P=2$ square law and $P=5/2$ power law. Both power laws accurately describe the data just above threshold, but the 5/2 power law fits better over a larger range than the square law. This indicates a $\sqrt{E}$ dependence in the transmission function for small E as predicted by the model. Still, the more complete the $T(E)$ model—which goes beyond the simple $\sqrt{E}$ approximation to the transmission function—always produces the best fit. The stability of the $T(E)$ model fits clearly demonstrates that the energy dependence of the electron transmission is well described by this semiclassical model over a substantial range of energy.

Finally, the effect of an energy-dependent mass was incorporated into the model. The energy-dependent mass was assumed to follow the relation $m^*(E)=m_0^*(1+\alpha E)$, where m_0^* is the value of the effective mass at the conduction-band minimum and α is the mass nonparabolicity factor.[32] For Si, the value $\alpha=0.5\ \mathrm{eV}^{-1}$ typically used is an average density of states value and does not directly describe the energy dependence for ballistic carriers. To account for this and to provide a bound on the magnitude of the effect on the simulation, all permutations of the longitudinal and transverse nonparabolicity factors, $\alpha_{\parallel}$ and α_t, with values 0 and 0.5 were investigated. The results are presented in Fig. 13 where the error vs fit range for each combination of parameters is plotted. All of the simulations were calculated using the $T(E)$ model, an isotropic electron distribution ($s=1.0$), and were fit to the BEES spectra taken on Au/Si(100) at 77 K. It is clear from Fig. 13 that the effect of an energy-dependent mass within the threshold region is very small. All of the simulations provide a good description of the data over approximately the same range. From this we conclude that the eventual

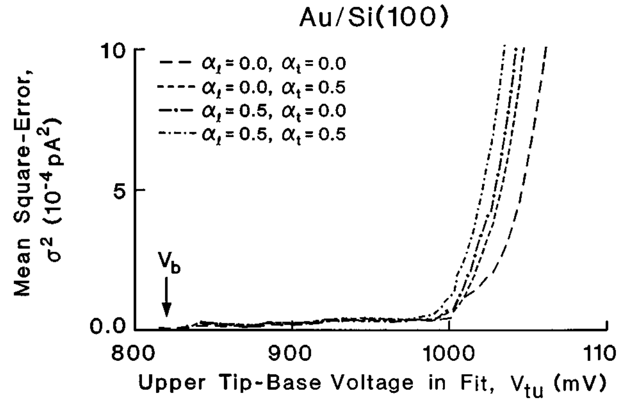

FIG. 13. The effect of an energy-dependent effective mass was investigated by fitting the data with simulations [$T(E)$ model] calculated using different combinations of longitudinal and transverse nonparabolicity factors, $\alpha_{\parallel}$ and α_t. All of the simulations provide a similar description of the data over approximately the same range, indicating that the effect of an energy-dependent mass within the threshold region is very small.

failure of the model at higher energies is not due exclusively to the nonparabolicity of the conduction band.

IV. CONCLUSION

From low-temperature BEES measurements on three different material systems, it was determined that a ballistic model which includes only the kinematical constraints of energy and momentum conservation does not adequately describe the experimental spectra. We have presented a semiclassical ballistic model that incorporates two of the most important dynamical effects in the transmission process. These are elastic scattering in the base or at the interface, and the quantum transmittance arising from the impedance mismatch for electron waves crossing the interface. The required form of the quantum transmittance was determined for electron transmission through nondegenerate conduction-band states between arbitrary materials. Model fits to the experimental spectra show that the inclusion of elastic scattering alone is also not sufficient to model accurately the BEES current in the near-threshold region (see $T=1$ model fits in Figs. 7–12). In contrast to this, the full $T(E)$ ballistic model—which includes the quantum transmittance—accurately models the shape of the experimental spectra over a substantial energy range for all three material interfaces. In addition, $T(E)$ model fits were consistently better than simple power-law approximations to the spectral shape. These conclusions were found to remain valid after including the effect of nonparabolic energy bands. We note that the range of validity is largest for Au/GaAs(100), which has the simplest electronic structure and is important for heterostructure devices.

ACKNOWLEDGMENTS

Helpful discussions with Dr. M. D. Stiles are acknowledged. This research was supported in part by the Joint Services Electronics Program under Grant No. DAAL-04-93-G-0027, the National Science Foundation under Grant Nos. ECS-9111866 and DMR-9223684, and the Office of Naval Research under Grant No. N00014-93-1-0475. D.K.G. gratefully acknowledges support from the NSF and G.N.H. acknowledges support received from the ONR.

---

[*] Present Address: M/A-COM, Inc., 100 Chelmsford St., P.O. Box 3294, Lowell, MA 01853-3294

[1] G. N. Henderson, P. N. First, T. K. Gaylord, and E. N. Glytsis, Phys. Rev. Lett. **71**, 2999 (1993).

[2] G. N. Henderson, T. K. Gaylord, E. N. Glytsis, P. N. First, and W. J. Kaiser, Solid State Commun. **80**, 591 (1991).

[3] A. E. Fowell, R. H. Williams, B. E. Richardson, A. A. Cafolla, D. I. Westwood, E. M. W. Anastassakis, and J. D. Joannopoulos, J. Vac. Sci. Technol. B **9**, 581 (1991).

[4] T. Sajoto, J. J. O'Shea, S. Bhargava, D. Leonard, M. A. Chin, and V. Narayanamurti, Phys. Rev. Lett. **74**, 3427 (1995).

[5] W. J. Kaiser and L. D. Bell, Phys. Rev. Lett. **60**, 1406 (1988).

[6] L. D. Bell and W. J. Kaiser, Phys. Rev. Lett. **61**, 2368 (1988).

[7] L. D. Bell, W. J. Kaiser, M. H. Hecht, and L. C. Davis, J. Vac. Sci. Technol. B **9**, 594 (1991).

[8] M. D. Stiles and D. R. Hamann, J. Vac. Sci. Technol. B **9**, 2394 (1991).

[9] P. Niedermann, L. Quattropani, K. Solt, A. D. Kent, and O. Fischer, J. Vac. Sci. Technol. B **10**, 580 (1992).

[10] R. Coratger, F. Ajustron, and J. Beauvillain, J. Phys. (France) III **3**, 2211 (1993).

[11] H. Palm, M. Arbes, and M. Schulz, Appl. Phys. A **56**, 1 (1993).

[12] A. A. Talin, D. A. A. Ohlberg, R. S. Williams, P. Sullivan, I. Koutselas, B. Williams, and K. L. Kavanagh, Appl. Phys. Lett. **62**, 2965 (1993).

[13] L. D. Bell and W. J. Kaiser, Scanning Microsc. **2**, 1231 (1988).

[14] R. Ludeke and A. Bauer, Phys. Rev. Lett. **71**, 1760 (1993).

[15] A. Fernandez, H. D. Hallen, T. Huang, R. A. Buhrman, and J. Silcox, Phys. Rev. B **44**, 3428 (1991).

[16] L. J. Schowalter and E. Y. Lee, Phys. Rev. B **43**, 9308 (1991).

[17] E. Y. Lee and L. J. Schowalter, J. Appl. Phys. **70**, 2156 (1991).

[18] H. D. Hallen, A. Fernandez, T. Huang, J. Silcox, and R. A. Buhrman, Phys. Rev. B **46**, 7256 (1992).

[19] R. Ludeke, J. Vac. Sci. Technol. A **11**, 786 (1993).

[20] R. Ludeke, Phys. Rev. Lett. **70**, 214 (1993).

[21] P. Niedermann, L. Quattropani, K. Solt, I. Maggio-Aprile, and O. Fischer, Phys. Rev. B **48**, 8833 (1993).

[22] A. Bauer and R. Ludeke, Phys. Rev. Lett. **72**, 928 (1994).

[23] G. N. Henderson, T. K. Gaylord, and E. N. Glytsis, Proc. IEEE **79**, 1643 (1991).

[24] M. Altarelli, Band structure, impurities and excitons in superlattices, in *Heterojunctions and Semiconductor Superlattices*, edited by G. Allan, G. Bastard, N. Boccara, M. Lannoo, and M. Voos (Springer-Verlag, Berlin, 1985), pp. 12–37.

[25] R. M. Kolbas, Y. C. Lo, and J. H. Lee, IEEE J. Quantum. Electron. **26**, 25 (1990).

[26] J. M. Luttinger and W. Kohn, Phys. Rev. B **97**, 869 (1955).

[27] S.-L. Chuang, Phys. Rev. B **40**, 10 379 (1989).

[28] G. N. Henderson, P. N. First, T. K. Gaylord, E. N. Glytsis, B. J. Rice, P. L. Dantzscher, D. K. Guthrie, L. E. Harrell, and J. S. Cave, Rev. Sci. Instrum. **66**, 91 (1995).

[29] A. A. Talin, R. S. Williams, and K. L. Kavanagh, in *Semiconductor Heterostructures for Photonic and Electronic Applications*, edited by C. W. Tu, D. C. Houghton, and R. T. Tung, MRS Symposia Proceedings No. 281 (Materials Research Society, Pittsburgh, 1993), p. 653.

[30] E. Y. Lee, B. R. Turner, L. J. Schowalter, and J. R. Jimenez, J. Vac. Sci. Technol. B **11**, 1579 (1993).

[31] F. J. Garcia-Vidal, P. L. de Andres, and F. Flores, Phys. Rev. Lett. **76**, 807 (1996).

[32] J. Singh, *Physics of Semiconductors and their Heterostructures* (McGraw-Hill, New York, 1993).